



# Comparison of by-product gas composition by activations of activated carbon

Gi Bbum Lee<sup>1</sup> · Jung Eun Park<sup>1</sup> · Sang Youp Hwang<sup>1</sup> · Ji Hyun Kim<sup>1</sup> · Seokhwi Kim<sup>1</sup> · Ho Kim<sup>1</sup> · Bum Ui Hong<sup>1</sup>

Received: 1 June 2018 / Accepted: 11 June 2018 / Published online: 9 March 2019  
© Korean Carbon Society 2019

## Abstract

In this study, commercial activated carbons (ACs) were upgraded by different activation methods, and the gases generated during the activations were defined and quantified. The chemical activation commonly applied for upgrading ACs uses complex reactions, involving pyrolysis, physical, and chemical reactions. The ACs based on wood materials were characterized by elemental analysis, N<sub>2</sub> physisorption, Fourier-transform infrared spectroscopy, X-ray photoelectron spectroscopy, and temperature-programmed desorption mass spectrometry. The patterns and composition of the generated gases were analyzed by gas chromatography and X-ray diffraction; high-resolution scanning electron microscopy was also used to characterize the activated carbon. The AC was mostly decomposed to CO<sub>2</sub> by pyrolysis and physical activation, while CO was mainly detected during chemical activation from the K<sub>2</sub>CO<sub>3</sub> produced by the reactions between CO<sub>2</sub> and K<sub>2</sub>O. The detected amounts of generated gases were differed at various KOH ratios and residence times. The highest surface area obtained in this study was 2000 m<sup>2</sup>/g at the optimum ratio of AC and KOH (1:2).

**Keywords** Activated carbon · Potassium hydroxide · Pyrolysis · Physical activation · Chemical activation · Gas

## 1 Introduction

Activated carbons (ACs) are widely used to adsorb and remove gaseous and liquid contaminants from pollutants because of their microporous structures and relatively large specific surface areas [1, 2]. Approximately 25% of commercial AC is used to remove gaseous substances, while the remaining 75% is used to treat liquid substances. AC for gas-phase adsorption is used to remove industrial gas emissions, recover pollution from the environment, and purify useful components. To facilitate the adsorption of gas pollutants, it is appropriate to use AC with well-developed micropores and a large specific surface area [3–5]. However, the specific surface area of commercial AC is limited for use in automobile applications, such as exhaust filters and canisters that adsorb highly concentrated pollutants in limited spaces. To overcome this spatial limitation, it is necessary to develop ACs with specific surface areas exceeding that of commercial ACs [6]. In addition, the generation of ACs with high

surface areas from commercial ACs is better than that from raw carbonaceous materials. Commercial ACs with low surface areas (~1500 m<sup>2</sup>/g) are inexpensive, but the product value can be significantly increased by enhancing the surface areas through activation. In addition, the yields of produced ACs by the activation of raw carbonaceous materials are extremely low. For those reasons, commercial ACs are currently used as starting materials for ACs with enhanced surface areas.

Studies are currently underway to increase specific surface areas through additional physical or chemical activation processes in an effort to make ACs with large specific surface areas. Physical activation is one method of increasing the specific surface area using water vapor and carbon dioxide as activators in an oxidizing atmosphere at high temperature (1000–1200 °C). One drawback of this method is the low C yield because of high C consumption in the oxidizing atmosphere. Meanwhile, chemical activation can obtain AC with large specific surface areas while consuming less C than physical activation does. This is because the chemical reaction oxidizes the C on the surface of ACs through chemical processing in an inert atmosphere at a relatively low temperature (600–900 °C) [4].

✉ Bum Ui Hong  
buhong@iae.re.kr

<sup>1</sup> Department of Plant Engineering, Institute for Advanced Engineering, Yongin 17180, Korea

Of the two aforementioned methods, the activation method using chemical activators (NaOH, KOH, etc.) is mainly used for the production of ACs with well-developed micropores and large specific surface areas, suitable for the adsorption of gaseous substances. Although the preparation of AC with large specific surface areas using this method has already been reported, few studies have investigated the activation mechanism and pore development [7–10]. The common method for the study of these mechanisms is to observe the generated gases during certain temperature intervals and matching them with possible reaction equations. Punsuwan et al. [11] examined the changes in specific surface area by activating palm kernels using various KOH ratios and analyzing the gases by gas chromatography (GC). In addition, Alcaniz-Monge et al. and Lillo-Rodenas et al. confirmed the various generated gases during the activation process using NaOH and KOH through temperature-programmed desorption (TPD) analysis [12, 13]. Existing studies on the gases generated during the chemical activation of ACs have not extended beyond simply analyzing the gas generation tendency or relating them to associated chemical reaction equations. However, gas analysis alone does not clearly demonstrate the activation mechanism, because the reactions during the activation process are not simple but complex, involving various processes and multiple variables. In the activation process using chemical activators, for example, steam and  $\text{CO}_2$  are generated, which also cause physical activation. Therefore, chemical activation cannot be separated from physical activation; activation must be considered as both chemical and physical.

The purpose of this study is to clarify the effects of activation methods by analyzing the generated gases during chemical activation, and considering pyrolysis and physical activation simultaneously.

## 2 Experimental

### 2.1 Materials

A wood-based AC (Brunauer–Emmett–Teller (BET) specific surface area:  $1400 \text{ m}^2/\text{g}$ ) referred to in this study as AC-R was used as the raw material, and KOH (potassium hydroxide, Samchun Chem. Co., 95%) was used as a chemical activation agent. After activation, 1 M of  $\text{H}_2\text{SO}_4$  (sulfuric acid, Samchun Chem. Co., 95%) was used as an agent to neutralize the remaining K compounds in the sample.

### 2.2 Experimental methods

Before all reactions, all samples were dried at  $100 \text{ }^\circ\text{C}$  for 6 h. A continuous-flow fixed-bed reactor was used for activation process. The reactor was charged with 1.0 g of AC-R, and then purged with high-purity  $\text{N}_2$  (99.999%). The vaporized K and water during the process were collected using a two-stage trap at the reactor outlet. Gas flow meters were also installed next to the traps to check the flow rate of the feed and product, as shown in Fig. 1. The ramping rate was  $5 \text{ }^\circ\text{C}/\text{min}$ , and the samples were held at  $750 \text{ }^\circ\text{C}$  for 1 h and then  $850 \text{ }^\circ\text{C}$  for 3 h for the activation process. The flow rates of  $\text{N}_2$  gas were changed to 100 mL/min, 50 mL/min, and 10 mL/min to observe the effect of flow rate. The ACs that were only heated for pyrolysis are denoted AC-H. To verify the effect of physical activation, the amount of water that could be theoretically produced from the reaction of AC and KOH (1:2) was mixed and reacted with AC-R. The sample reacted with water is referred to as AC-W. Chemical activation was performed at different weight ratios of AC and KOH (1:1, 1:2, and 1:3), and these are referred to as AC-1K, AC-2K, and AC-3K according to the ratio of the activation agent. The neutralized samples were then washed to pH 7

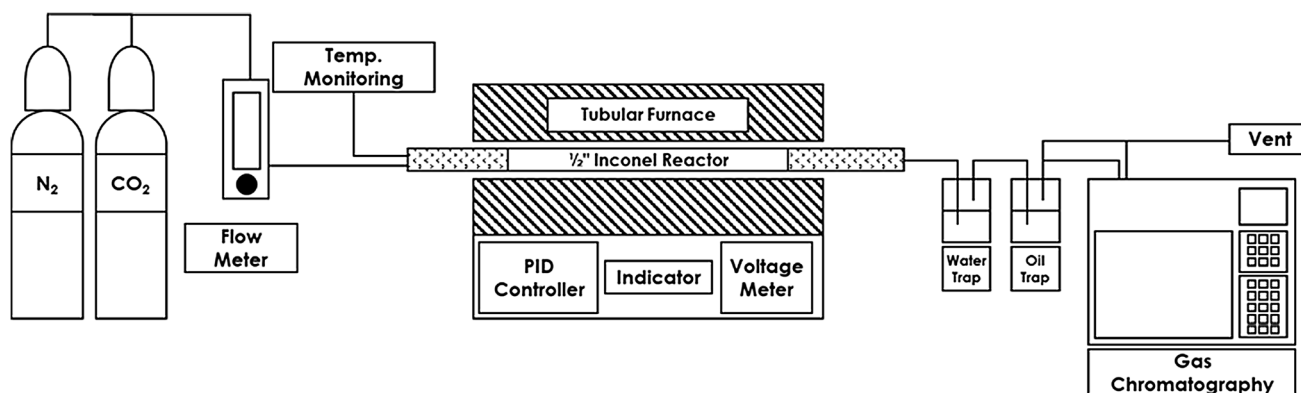


Fig. 1 Schematic diagram of activation reactor

with distilled water. After washing, samples were dried in a 100 °C oven and subjected to various analyses.

### 2.3 Analysis

The AC-R used in the activation reaction was subjected to the following basic analysis. For the proximate analysis, dried samples were placed in the furnace (Furnace, Daehung science, DF-4S) and then heated at 950 °C for 7 min and then 750 °C for 10 h, respectively. The results, including the ash, volatile, and fixed-carbon contents within the ACs, were considered as percentages of the weight (Table 1). Elemental analysis (EA) was performed for 12 min at 900 °C using an elemental analyzer (Thermo Scientific, FlashEA 1112) to determine the elemental contents of C, H, O, N, and S. The content of oxygen functional groups on the surface was confirmed by X-ray photoelectron spectroscopy (XPS, Thermo Scientific, VG Multilab 2000). Carbon bonds and oxygen groups were also qualitatively confirmed via the attenuated total reflectance (ATR) method using Fourier-transform infrared (FT-IR) spectroscopy (Thermo Scientific, Nicolet 6700). Those functional groups caused the gas generations from the pyrolysis reaction. The TPD was performed using an Autochem 2910 unit (Micromeritics) and the product gas was measured with an online mass spectrometer (QMS 200, Pfeiffer Vacuum). Generally, a quartz U-tube reactor was loaded with 0.10 g of samples, and the samples were analyzed by continuously raising the temperature from 40 to 900 °C at 10 °C intervals, and then held at the temperature for 1 h. GC (HP 6890, Agilent) was employed for the quantitative analysis of the generated gases during the activation reaction, followed by thermal conductivity detector (TCD) analysis performed using a packed column (ShinCarbon ST, RESTEK). After the reaction, the

changes in the properties and quantity of the K residue were confirmed using an X-ray diffraction (XRD) analyzer (SHIMADZU, XRD-6100). In addition, the samples were analyzed by high-resolution scanning electron microscopy (HR-SEM; Hitachi High-Tech, SU 8010) to observe the surface structure changes in the raw and activated ACs. The specific surface areas and pore distributions were measured by the BET and Barrett–Joyner–Halenda (BJH) methods based on the N<sub>2</sub> adsorption data obtained at 77 °C using an adsorption analyzer (ASAP-2010, Micromeritics).

### 3 Results and discussion

As shown in Table 1, proximate and elemental analyses were performed to confirm the composition of AC-R.

The results show the initial O contents of AC-R, which is relative volatile in content. Generally, the wood-based AC is higher in O than coconut- or coal-based AC [10, 11, 14]. This is expected to affect the formation of micropores through the oxidation–reduction reaction of the activators upon activation. Molina-Sabio and Rodríguez-Reinoso noted that micropores are generated by the sustained oxidation–reduction reaction of the activators [15].

The results of EA of the produced materials are shown in Table 1. The pyrolysis (AC-H) and physical activation (AC-W) cause the decrease of O contents, so the relative C composition is increased. The chemical activation slightly decreases the C composition as the ratio of AC and KOH is increased, while the H and O contents are increased, suggesting the increase of hydroxyl groups. As the ratio of AC and KOH is increased, the pattern of H and O also increases, as with the previous report [16].

**Table 1** Proximate and elemental analysis of wood base activated carbon samples

Proximate analysis (wt%)					
	Volatile		Fixed carbon		Ash
AC-R	20.9		72.7		6.4
Elemental analysis (wt%)					
	C	H	O	N	S
AC-R	68.8	0.96	15.7	0.27	0.12
AC-H	83.0	1.10	5.77	0.28	N.D.
AC-W	88.7	0.72	2.74	0.24	N.D.
AC-1K	84.5	0.34	4.30	0.95	N.D.
AC-2K	80.6	0.53	6.37	2.56	N.D.
AC-3K	74.8	0.74	6.50	0.27	N.D.

Analysis condition: dry basis

AC-R raw material, AC-H heated for pyrolysis, AC-W reacted with water, AC-1K AC-R/KOH ratio = 1, AC-2K AC-R/KOH ratio = 2, AC-3K AC-R/KOH ratio = 3, respectively

The O-containing functional groups on the surfaces of the ACs were analyzed by FT-IR and XPS. The results of FT-IR analysis in Fig. 2a show C=O–C bonds in ether structures and hydroxyl groups at around  $1050\text{ cm}^{-1}$ , the C=C bonds in aromatic structures at around  $1550\text{ cm}^{-1}$ , C=O bond corresponding to the quinone series or carboxylic acids at around  $1650\text{--}1860\text{ cm}^{-1}$ , C≡C bonds at  $2100\text{ cm}^{-1}$ , and the –OH bonds of phenol groups at  $3429\text{ cm}^{-1}$  [17, 18].

Figure 2b shows the C 1s XPS spectrum of AC-R. Depending on the samples, the curves are deconvoluted into five peaks. In brief, the C 1s XPS spectrum of AC-R shows the presence of significant oxidation, with five components corresponding to C atoms in various functional groups, including oxygenated ring C=C ( $sp^2$ ), C–C ( $sp^3$ ), C–O, C=O, and –COOH bonding at 284.4, 285.5, 286.4, 287.7, and 289.3 eV, respectively. The contents in the samples are 65.7%, 16.7%, 9.3%, 5.0%, and 3.3%, respectively, indicating that AC-R has a variety of O-containing functional groups on the surface such as phenol, quinone, ether, carbonyl, and carboxyl groups, as confirmed by FT-IR analysis [19].

The TPD curves for  $\text{H}_2\text{O}$ ,  $\text{CO}_2$ , and CO evolution from the AC-R are shown in Fig. 2c. The peak detected at approximately  $77\text{ }^\circ\text{C}$  is related to  $\text{H}_2\text{O}$  and attributed to the transformation of a pair of –COOH functional groups into the anhydride form [20]. As shown in Fig. 2c inset,  $\text{CO}_2$  is generated at approximately  $177\text{ }^\circ\text{C}$ , because of the decomposition of carboxylic groups. At temperatures of  $400\text{--}600\text{ }^\circ\text{C}$ , peaks associated with  $\text{CO}_2$  and CO are observed, suggesting the decomposition of carboxylic acid anhydride and oxygen surface groups. The peaks related to  $\text{CO}_2$  and CO are detected again at approximately  $777\text{ }^\circ\text{C}$ . This is caused by the decomposition of the carbonyl groups [21]. The total desorption amount of CO and  $\text{CO}_2$  is  $4250\text{ }\mu\text{mol/g}$ .

The pyrolysis reaction was performed for 1 h at  $750\text{ }^\circ\text{C}$  and for 3 h at  $850\text{ }^\circ\text{C}$  at a heating rate of  $5\text{ }^\circ\text{C/min}$ , after

purging the sample, which was pre-dried for over 6 h, for 30 min in the  $1/2''$  reactor filled with  $\text{N}_2$  gas.

The generated CO and  $\text{CO}_2$  by pyrolysis were caused by the decomposition of O-containing functional groups on the carbon surface [21].

Oxygen functional group  $\rightarrow$  CO or  $\text{CO}_2$  (1)

Here,  $\text{H}_2\text{O}$  participating in the reaction is believed to arise from anhydride, which formed by carboxylic acid dehydration, as mentioned in the TPD-MS analysis results shown in Fig. 2c.

For AC-H,  $63.5\text{ }\mu\text{mol}$  of  $\text{H}_2$  gas was generated in the temperature range between  $25\text{ }^\circ\text{C}$  and  $750\text{ }^\circ\text{C}$ , and then  $308\text{ }\mu\text{mol}$  was generated over  $750\text{--}850\text{ }^\circ\text{C}$ .  $302\text{ }\mu\text{mol}$  of CO gas was generated at temperatures up to  $750\text{ }^\circ\text{C}$ ; an additional  $386\text{ }\mu\text{mol}$  was generated over  $750\text{--}850\text{ }^\circ\text{C}$  by surface functional group decomposition. The generation pattern of CO gas was similar to that for  $\text{H}_2$  gas. In the case of  $\text{CH}_4$  gas,  $5.26\text{ }\mu\text{mol}$  is detected, which is relatively small compared to other gases, but the generation pattern is the same as that for other gases. Van Heek et al. [22] also reported that steam affects  $\text{CH}_4$  generation, which is explained as part of gasification. The  $4371\text{ }\mu\text{mol}$  (total) of  $\text{CO}_2$  gas is generated by the thermal decomposition of carboxyl groups on the AC surface.

In AC-W,  $\text{H}_2$  gas is formed by the water–gas reaction (WGR) and water–gas shift reaction (WGSR), as shown in Eqs. (2) and (3), respectively [23, 24].



Approximately  $24.9\text{ }\mu\text{mol}$   $\text{H}_2$  gas is generated between  $25$  and  $750\text{ }^\circ\text{C}$ , with an additional  $397\text{ }\mu\text{mol}$  generated in the range  $750\text{--}850\text{ }^\circ\text{C}$ .  $277\text{ }\mu\text{mol}$  of CO gas is generated in the temperature range up to  $750\text{ }^\circ\text{C}$  by surface functional

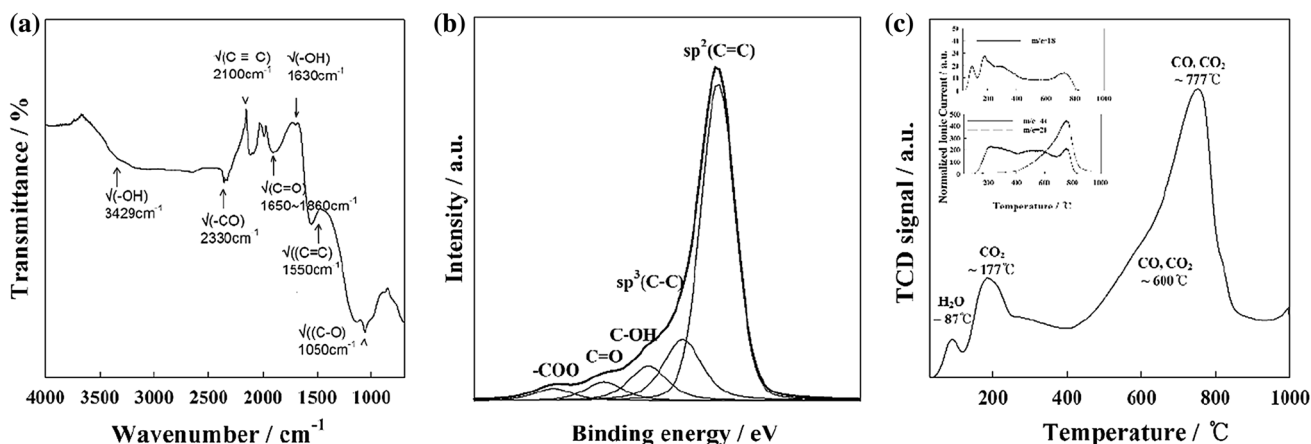
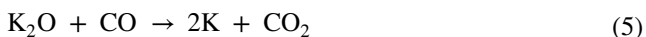


Fig. 2 Analysis results of AC-R a FT-IR spectra, b XPS spectra, and c TPD-Mass, respectively

group decomposition. In addition, 354  $\mu\text{mol}$  of  $\text{CO}$  gas was generated over the range 750–850  $^{\circ}\text{C}$ . The total 7950  $\mu\text{mol}$  of  $\text{CO}_2$  was generated according to Eq. (3). In the case of  $\text{CH}_4$  gas, 9.98  $\mu\text{mol}$  is detected.

Chemical activation was performed using  $\text{KOH}$  as an activator for AC-R with the temperature conditions and flow rates maintained as above. The  $\text{KOH}$  used as the activator is converted to  $\text{K}_2\text{O}$  and  $\text{H}_2\text{O}$ , thereby facilitating both physical and chemical activations simultaneously, as shown in Eq. (3). Because the weight ratio with AC is an important activation parameter, the generation pattern of activation gases was analyzed accordingly.

First, in the case of AC-1K, 28.4  $\mu\text{mol}$  and 5.0  $\mu\text{mol}$  of  $\text{H}_2$  gas are generated by WGR in the heating range and the WGSR in the activation range, respectively. The pattern of gas generation is shifted to lower temperatures than those in pyrolysis or physical activation, as shown in Fig. 3 (AC-1K). A study by Hsu and Teng also showed that the reaction for chemical activation starts at a lower temperature than that for pyrolysis [4]. As shown in Fig. 3 (AC-1K), 40.8  $\mu\text{mol}$  of  $\text{H}_2$  is generated at temperatures of < 750  $^{\circ}\text{C}$ , while 74.0  $\mu\text{mol}$  is generated in the activating range. The pattern for the amount of  $\text{CO}$  generation differs from that in pyrolysis and physical activation. The amount of  $\text{CO}$  generation in the activating range over 751  $^{\circ}\text{C}$  is larger than that in the initial stages at low temperatures. This is because  $\text{CO}$  gas is continuously generated through the reaction between  $\text{K}_2\text{O}$  and surface C, as shown in Eq. (4) [23]. The generated amount of  $\text{CH}_4$  gas was 0.24  $\mu\text{mol}$ , which is relatively small and shows a different pattern from pyrolysis and physical activation because of the effects of physical activation. It was expected that  $\text{CO}_2$  gas would be generated in large volumes by the surface O-containing functional groups, as shown in Eq. (5), or by reaction with  $\text{CO}$  gas generated through reactions with surface C, as shown in Eq. (4). However, no such results are observed in the gas analysis. It is also found that the overall chemical exhaustion is less than that in pyrolysis and physical activation, which will be discussed in more detail through the post-reaction sample analysis.



For AC-2K, it is confirmed that the amount of generated gas is more than twice that from AC-1K because of the increased  $\text{KOH}$  input. As shown in Fig. 3 (AC-2K),  $\text{H}_2$  gas is generated from the WGR and WGSR during the activation process. 98.4  $\mu\text{mol}$  of  $\text{H}_2$  is generated in the heating range, while 9.54  $\mu\text{mol}$  is generated in the activation range. In addition, 8.13  $\mu\text{mol}$  and 265  $\mu\text{mol}$  of  $\text{CO}$

are generated in the temperature regimes of heating and activating, respectively. The generation pattern of  $\text{CO}$  is similar to that of AC-1K, which is larger at higher temperatures than at lower temperatures. 1.06  $\mu\text{mol}$  of  $\text{CH}_4$  gas is also generated by physical activation factors, in the same manner as the aforementioned reactions.  $\text{CO}_2$  is not detected in AC-2K, similar to AC-1K.

A  $\text{H}_2$  gas generation pattern similar to those of weight ratio 1 and 2 is observed in the case of AC-3K, as shown in Fig. 3 (AC-3K).  $\text{H}_2$  gas shows the highest concentration at 527–727  $^{\circ}\text{C}$  with 113  $\mu\text{mol}$  generated and 3.73  $\mu\text{mol}$  in the activation range. In the case of  $\text{CO}$  gas, however, the generation temperature is shifted higher and the amount is slightly decreased. 0.53  $\mu\text{mol}$  and 150  $\mu\text{mol}$  of  $\text{CO}$  gas are generated in the heating range and activating range at 750–850  $^{\circ}\text{C}$ , respectively. 0.78  $\mu\text{mol}$  of  $\text{CH}_4$  gas is generated, while no  $\text{CO}_2$  is detected, similar to AC-1K and AC-2K.

The total amounts of gas generated in each reaction are shown in Table 2. The generation of  $\text{H}_2$  gas in both pyrolysis and physical activation is higher than that in chemically activated ACs. The amount from physical activation is relatively large because of water addition. However, the  $\text{H}_2$  amount generated is 422  $\mu\text{mol}$ , which is only 0.3% of the theoretically produced amount, when water is fully reacted during the reaction. In addition, the amount of  $\text{CO}$  gas generated should be increased by the water participating in the reaction, but the actual amount physically generated is less than that via pyrolysis, suggesting that sufficiently supplied water was involved in the WGSR in Eq. (2). This can be matched with the amount of generated  $\text{CO}_2$  gas. The production amount of  $\text{CH}_4$  gas is increased during the physical activation process, because of the increase of physical activation factors according to steam generation. The generated amount of  $\text{H}_2$  gas is smaller than that in pyrolysis and physical activation, but it tends to increase as the weight ratio increases [25]. The difference in the amount of produced  $\text{H}_2$  is caused by the type of supplied water. The water was directly injected in the physical activation, while the water was produced through the reaction of Eq. (3) above 227  $^{\circ}\text{C}$  during the chemical activation reaction. In the case of  $\text{CO}$  gas, the amount is increased as the weight ratio is increased from 1 (AC-1K) to 2 (AC-2K), but it is decreased again at the ratio of 3 (AC-3K). This is caused by the reaction of  $\text{K}_2\text{O}$  and  $\text{CO}$  in Eq. (5); then the  $\text{CO}_2$  produced from the reaction also reacts with  $\text{K}_2\text{O}$  again. An experiment was performed by controlling the flow rate of  $\text{N}_2$ , which was used as an inert gas, based on the AC-2K condition to observe the effect of the space velocity [26]. As shown in Fig. 4, the amount of  $\text{CO}$  gas generation is decreased as the flow rate decreases, because the generated  $\text{CO}$  gas is not removed and then consumed as a reactant. Such results are attributed to the aforementioned reactions in Eqs. (2) and (5). At higher flow rates, the generated by-product gas is easily removed,

**Fig. 3** Cumulative gas production of various activation results [H<sub>2</sub> (circle), CO (square), CH<sub>4</sub> (triangle), CO<sub>2</sub> (inverted triangle)]

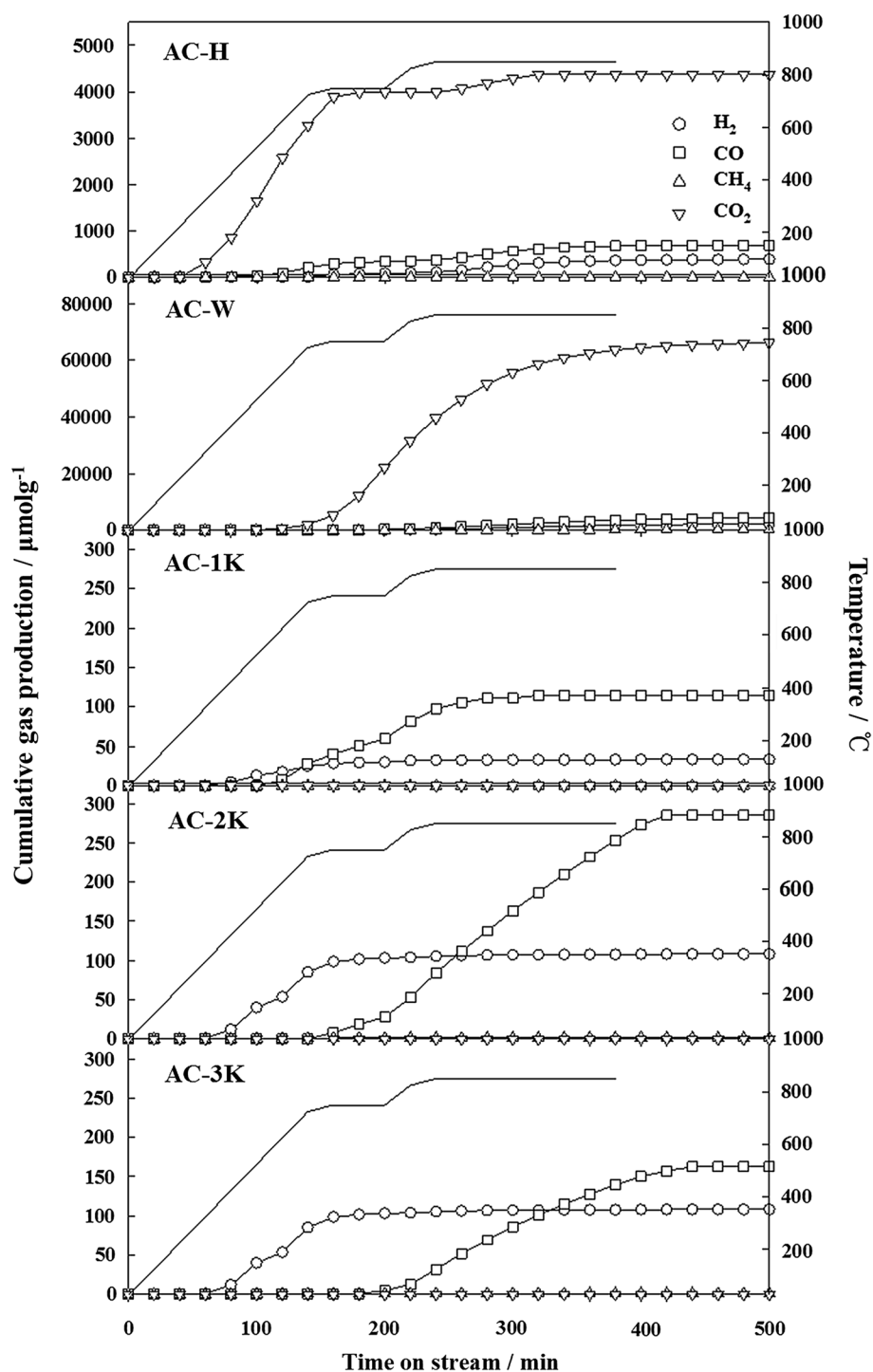


**Table 2** Cumulative gas production in activation reaction

Sample	H <sub>2</sub> (μmol/g)	CO (μmol/g)	CH <sub>4</sub> (μmol/g)	CO <sub>2</sub> (μmol/g)
AC-H	372	687	5.26	4370
AC-W	420	631	9.98	7950
AC-1K	33	115	0.24	N.D.
AC-2K	108	273	1.06	N.D.
AC-3K	117	150	0.78	N.D.

thus suppressing the side reactions during the activation reaction. When the supplied flow rates are 50 mL/min g and 100 mL/min g, the inert gas atmosphere can be maintained by the N<sub>2</sub> gas because the CO gas begins emission before 150 min. At the supply flow rate of 10 mL/min g, however, the produced CO is not removed and reacted with K<sub>2</sub>O in Eq. (5), so the K compounds from K<sub>2</sub>O do not participate in the main reaction, as in Eq. (4).

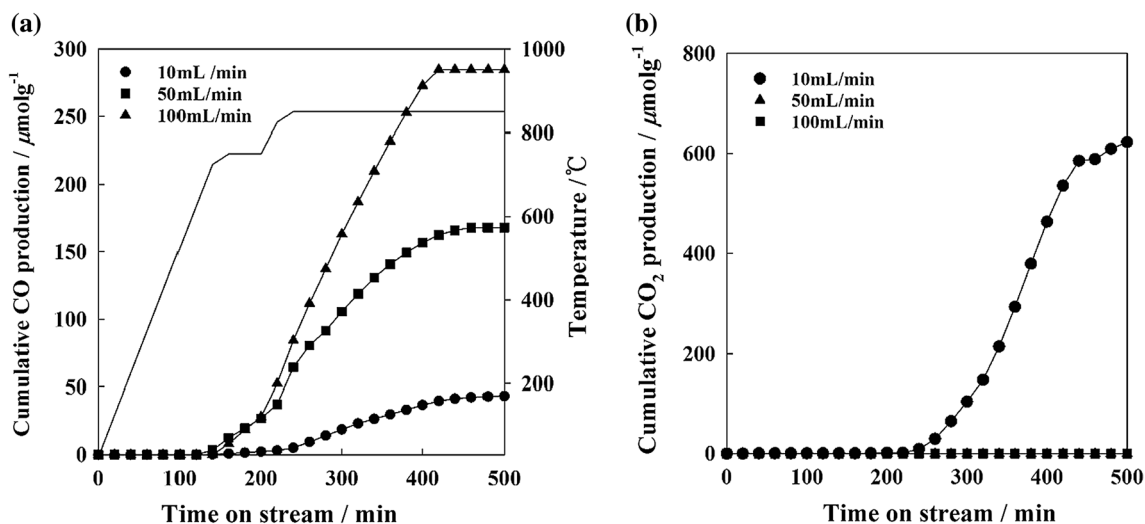


**Fig. 4** a CO cumulative production with different space velocity (circle) 10 mL/min g, (square) 50 mL/min g, (triangle) 100 mL/min g. b  $\text{CO}_2$  cumulative production (filled circle) at space velocity 10 mL/min g, respectively

BET, XRD, and SEM analyses were performed to investigate the characteristics of the AC after the reactions.

XRD analysis was performed using samples that had not been subjected to the washing process after activation. As shown in Fig. 5, the XRD patterns of ACs subjected to the pyrolysis (AC-H) and physical activation (AC-W) processes are similar with that of the raw material (AC-R), with broad peaks inherent to activated carbon confirmed as the (002) and (101) planes [27]. It has been reported that the amount of generated gas generally increased with increases in the amount of activator, but in this study, the amount of CO is decreased in the reaction with the activator ratio of 3, suggesting that CO was consumed during the activation process. As mentioned above, the generated CO was reacted with  $\text{K}_2\text{O}$  in Eq. (5), and the generated  $\text{CO}_2$  was reacted with  $\text{K}_2\text{O}$  in Eq. (6). As a result, Potassium carbonate (JCPDS:

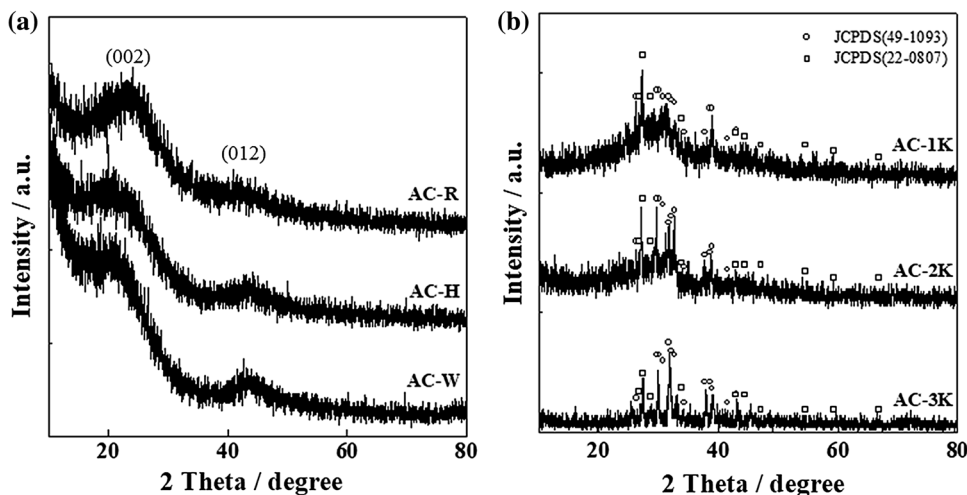
49-1093 and JCPDS: 22-0807) is formed during chemical activation [24].



XRD patterns for  $\text{K}_2\text{CO}_3$  are detected from all samples after chemical activations, as shown in Fig. 5b. The samples tend to show increased shares of  $\text{K}_2\text{CO}_3$  as the ratio of KOH increases after chemical activation. This is because the K residues present in the AC inhibit the gasification rate and the generation of  $\text{CO}_2$  gas [28].

HR-SEM analysis was performed after the activation reactions to confirm the changes in the surface characteristics of the ACs. As shown in Fig. 6, AC-R shows pores of  $\sim 100$  nm in size. As the pyrolysis and physical activation proceed, the overall size of pores is reduced to approximately 40–50 nm. It can be seen that a relatively greater

**Fig. 5** XRD spectra without washing a AC-R, AC-H, AC-W, b AC-1K, AC-2K, AC-3K



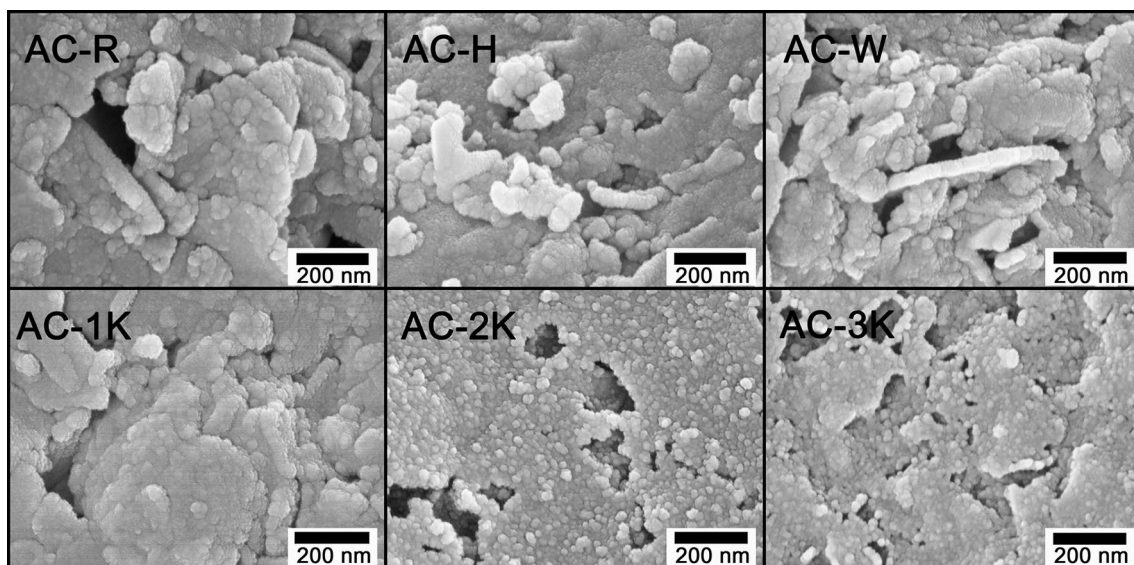


**Fig. 6** Image of high resolution scanning electron microscopy

number of fine pores (< 10 nm) is developed after chemical activation, and pores of < 100 nm are also developed as the activation ratio increases.

The specific surface areas of the ACs were analyzed to confirm the correlation between the generated gas and the specific surface area. Figure 7 shows the  $N_2$  adsorption–desorption isotherms and pore size distributions of the ACs. It is found that the ACs exhibit type-I and IV isotherms and the pore size distributions show three volcano-shape patterns. The position of the volcano-shape pattern for AC-R is similar to those for AC-H and AC-W. In the case of physical

activation, a total structural collapse occurs, given that the total micropore volume is reduced, thereby reducing the specific surface area. On the other hand, it can be seen that the specific surface area tends to increase with increasing KOH/AC ratio during chemical activation. When the KOH activation weight is increased, the slope of the isotherms gradually increases and the isotherms show hysteresis loops.

AC-R has an initial specific surface area of  $1398 \text{ m}^2/\text{g}$ , which is gradually reduced to  $1386 \text{ m}^2/\text{g}$  and  $1196 \text{ m}^2/\text{g}$  through pyrolysis and physical activation in Table 3, respectively. With pyrolysis, the total micropore volume does not

**Fig. 7** **a** Nitrogen adsorption and desorption isotherms and **b** pore width distributions of AC. Closed and open symbols are adsorption and desorption isotherm, respectively

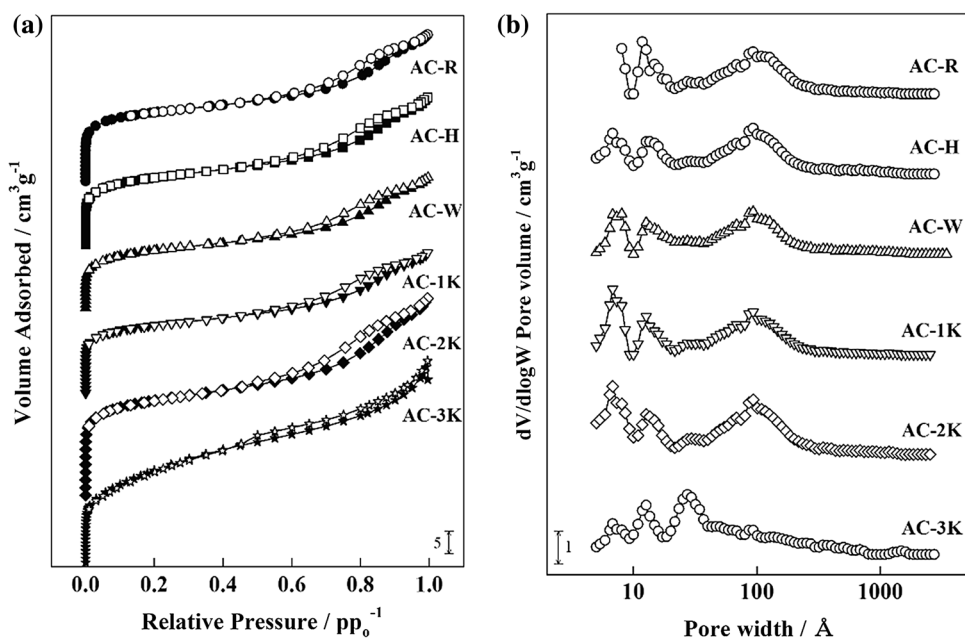




**Table 3** Physical properties of raw material and after activation

Sample	$S_{\text{BET}}$ (m <sup>2</sup> /g)	$D_p$ (nm)	$V_{\text{Total}}$ (cm <sup>3</sup> /g)	$V_{\text{Micro}}$ (cm <sup>3</sup> /g)	$R_{\text{Micro}}$
AC-R	1398	6.31	1.17	0.34	0.29
AC-H	1386	3.18	1.17	0.30	0.26
AC-W	1196	5.30	1.04	0.22	0.21
AC-1K	1409	4.79	1.18	0.36	0.30
AC-2K	2014	5.57	1.58	0.49	0.31
AC-3K	1916	4.26	1.46	0.40	0.28

change significantly, but the overall ratio is decreased as the micropores develop into mesopores [29]. This is attributed to the escape of oxygen functional groups such as  $\text{C}=\text{O}$  and  $\text{COO}$  in the existing micropore by pyrolysis or physical activation, which decreased the number of micropores of  $< 2$  nm and promoted mesopore formation of 2–50 nm.

The isotherm of AC-1K shows that the values of total micropore volume are increased compared to those of AC-R. Conversely, the mesopores are decreased by approximately 6%, significantly suppressing the increase in overall specific surface area. The isotherms of AC-2K and AC-3K show specific surface areas reduced by approximately 80 m<sup>2</sup>/g, which is attributed to the movement of micropores of  $< 1$  nm into mesopores measuring between 2 and 5 nm [30]. As a result, pyrolysis and physical activation seem to decrease the specific surface areas as the micropores collapse or the mesopore ratios are increased, rather than stimulating pore development. In addition, chemical activation increases the specific surface area by micropore development compared to physical activation.

## 4 Conclusions

In summary, we investigated gas generation occurring in the pyrolysis, physical activation, and chemical activation of ACs. Pyrolysis and physical activation mainly triggered the generation of CO<sub>2</sub> by the decomposition of O-containing functional groups. The amount of decomposed O-containing functional groups measured by TPD-MS is similar to that of the gases detected by GC. During the chemical activation, CO is mainly produced and the amount of generated gases is dependent on the ratio of ACs and KOH. However, K residues during the chemical activation suppress the emission of CO<sub>2</sub>. The reduced CO<sub>2</sub> emission indicates the reaction of K<sub>2</sub>O and CO<sub>2</sub>, which are stabilized in the form of potassium carbonate. The higher concentration of CO from AC-2K corresponds to larger specific surface areas, while the lower specific area of AC-3K corresponds to its low CO emissions. The results of gas generation patterns and concentrations can guide the development of specific surface area in ACs.

The residence time is also significant for maintaining inert atmospheres for the activation reaction, because sufficient flow rates can suppress other side reactions.

**Acknowledgements** This study was supported by the Energy Development Technology Program of the Korea Institute of Energy Technology Evaluation and Planning (KETEP) granted financial resource from the Ministry of Trade, Industry & Energy, republic of Korea (Project No. 20162010104680), and also the National Research Foundation of Korea (NRF) and the Center for Women In Science, Engineering and Technology (WISSET) Grant funded by the Ministry of Science and ICT under the Program for Returners into R&D.

## References

- Sudaryanto Y, Hartono SB, Irawaty W, Hindarso H, Ismadji S (2006) High surface area activated carbon prepared from cassava peel by chemical activation. *Biores Technol* 97:734–739. <https://doi.org/10.1016/j.biortech.2005.04.029>
- Cazetta AL, Vargas AMM, Nogami EM, Kunita MH, Guilherme MR, Martins AC, Silva TL, Moraes JCG, Almeida VC (2011) NaOH-activated carbon of high surface area produced from coconut shell: kinetics and equilibrium studies from the methylene blue adsorption. *Chem Eng J* 174:117–125. <https://doi.org/10.1016/j.cej.2011.08.058>
- Reimerink WMTM, Kleut Dvd (1999) Air pollution control by adsorption. *Stud Surf Sci Catal* 120:807–819. [https://doi.org/10.1016/S0167-2991\(99\)80380-2](https://doi.org/10.1016/S0167-2991(99)80380-2)
- Hsu LY, Teng H (2000) Influence of different chemical reagents on the preparation of activated carbons from bituminous coal. *Fuel Process Technol* 64:155–166. [https://doi.org/10.1016/S0378-3820\(00\)00071-0](https://doi.org/10.1016/S0378-3820(00)00071-0)
- Kyotani T (2000) Control of pore structure in carbon. *Carbon* 38:269–286. [https://doi.org/10.1016/S0008-6223\(99\)00142-6](https://doi.org/10.1016/S0008-6223(99)00142-6)
- Ghouma I, Jeguirim M, Sager U, Limousy L, Bennici S, Daber E, Asbach C, Ligotski R, Schmidt F, Ouederni A (2017) The potential of activated carbon made of agro-industrial residues in NOx immissions abatement. *Energies* 10:1508. <https://doi.org/10.3390/en10101508>
- AdibYahya M, Al-Qodah Z, ZanariahNgah CW (2015) Agricultural bio-waste materials as potential sustainable precursors used for activated carbon production: a review. *Renew Sustain Energy Rev* 46:218–235. <https://doi.org/10.1016/j.rser.2015.02.051>
- Carvalho AP, Cardoso B, Pires J, Carvalho MB (2003) Preparation of activated carbons from cork waste by chemical activation with KOH. *Carbon* 41:2873–2884. [https://doi.org/10.1016/S0008-6223\(03\)00323-3](https://doi.org/10.1016/S0008-6223(03)00323-3)
- Li XF, Xu Q, Fu Y, Guo QX (2013) Preparation and characterization of activated carbon from kraft lignin via KOH activation. *Environ Prog Sustain Energy* 33:519–526. <https://doi.org/10.1002/ep11794>
- Hayashi J, Kazehaya A, Muroyama K, Watkinson AP (2000) Preparation of activated carbon from lignin by chemical activation. *Carbon* 38:1873–1878. [https://doi.org/10.1016/S0008-6223\(00\)00027-0](https://doi.org/10.1016/S0008-6223(00)00027-0)
- Punsuwan N, Tangsathitkulchai C, Takarada T (2015) Low temperature gasification of coconut shell with CO<sub>2</sub> and KOH: effects of temperature, chemical loading, and introduced carbonization step on the properties of syngas and porous carbon product. *Int J Chem Eng* 25:16. <https://doi.org/10.1155/2015/481615>
- Alcañiz-Monge J, Illán-Gómez MJ (2008) Insight into hydroxides-activated coals: Chemical or physical activation? *J Colloid Interface Sci* 318:35–41. <https://doi.org/10.1016/j.jcis.2007.10.017>

13. Lillo-Ródenas MA, Cazorla-Amorós D, Linares-Solano A (2003) Understanding chemical reactions between carbons and NaOH and KOH: an insight into the chemical activation mechanism. *Carbon* 41:267–275. [https://doi.org/10.1016/S0008-6223\(02\)00279-8](https://doi.org/10.1016/S0008-6223(02)00279-8)
14. Sun P, Zhang B, Zeng X, Luo G, Li X, Yao H, Zheng C (2017) Deep study on effects of activated carbon's oxygen functional groups for elemental mercury adsorption using temperature programmed desorption method. *Fuel* 200:100–106. <https://doi.org/10.1016/j.fuel.2017.03.031>
15. Molina-Sabio M, Rodríguez-Reinoso F (2004) Role of chemical activation in the development of carbon porosity. *Colloids Surf A Physicochem Eng Asp* 241:15–25. <https://doi.org/10.1016/j.colsurfa.2004.04.007>
16. Kumar A, Jena HM (2016) Preparation and characterization of high surface area activated carbon from Fox nut (*Euryale ferox*) shell by chemical activation with H<sub>3</sub>PO<sub>4</sub>. *Results Phys* 6:651–658. <https://doi.org/10.1016/j.rinp.2016.09.012>
17. Tucureanu V, Matei A, Avram AM (2016) FTIR spectroscopy for carbon family study. *Crit Rev Anal Chem* 46:502–520. <https://doi.org/10.1080/10408347.2016.1157013>
18. Alzaydien AS (2016) Physical, chemical and adsorptive characteristics of local oak sawdust based activated carbon. *Asian J Sci Res* 9:45–56. <https://doi.org/10.3923/ajsr.2016.45.56>
19. Terzyk AP (2001) The influence of activated carbon surface chemical composition on the adsorption of acetaminophen (paracetamol) in vitro Part II. TG, FTIR, and XPS analysis of carbons and the temperature dependence of adsorption kinetics at the neutral pH. *Colloids Surf A Physicochem Eng Asp* 177:23–45
20. Roberts JD, Caserio MC (1977) Basic principles of organic chemistry, 2nd edn. W. A. Benjamin, Inc., Menlo Park, p 847. ISBN 0-8053-8329-8
21. Li N, Ma X, Zha Q, Kim K, Chen Y, Song C (2011) Maximizing the number of oxygen-containing functional groups on activated carbon by using ammonium persulfate and improving the temperature-programmed desorption characterization of carbon surface chemistry. *Carbon* 49:5002–5013. <https://doi.org/10.1016/j.carbon.2011.07.015>
22. Van Heek KH, Juentgen H, Peters W (1973) Fundamental studies on coal gasification in the utilization of thermal energy from nuclear high temperature reactors. *J Inst Fuel* 46:249–258
23. Wigmans T, Elfring R, Moulijn AJ (1983) On the mechanism of the potassium carbonate catalysed gasification of activated carbon: the influence of the catalyst concentration on the reactivity and selectivity at low steam pressures. *Carbon* 21:1–12. [https://doi.org/10.1016/0008-6223\(83\)90150-1](https://doi.org/10.1016/0008-6223(83)90150-1)
24. Romanos J, Beckner M, Rash T, Firlj L, Kuchta B, Yu P, Suppes G, Wexler C, Pfeifer P (2012) Nanospace engineering of KOH activated carbon". *Nanotechnology* 23:1–7. <https://doi.org/10.1088/0957-4484/23/1/015401>
25. Lozano-Castello D, Calo JM, Cazorla-Amorós D, Linares-Solano A (2007) Carbon activation with KOH as explored by temperature programmed techniques, and the effects of hydrogen. *Carbon* 45:2529–2536. <https://doi.org/10.1016/j.carbon.2007.08.021>
26. Fierro V, Torné-Fernández V, Celzard A (2007) Methodical study of the chemical activation of Kraft lignin with KOH and NaOH. *Microporous Mesoporous Mater* 101:419–431. <https://doi.org/10.1016/j.micromeso.2006.12.004>
27. Liu XY, Huang M, Ma HL, Zhang ZQ, Gao JM, Zhu YL, Han XJ, Guo XY (2010) Preparation of a carbon-based solid acid catalyst by sulfonating activated carbon in a chemical reduction process. *Molecules* 15:7188–7196. <https://doi.org/10.3390/molecules15107188>
28. Moreno-Piraján JC, Bastidas-Barranco MJ, Giraldo L (2018) Preparation of activated carbons for storage of methane and its study by adsorption calorimetry. *J Therm Anal Calorim* 131:259–271. <https://doi.org/10.1007/s10973-017-6132-8>
29. Rodríguez-Reinoso F, Molina-Sabio M (1992) Activated carbons from lignocellulosic materials by chemical and/or physical activation: an overview. *Carbon* 30:1111–1118. [https://doi.org/10.1016/0008-6223\(92\)90143-K](https://doi.org/10.1016/0008-6223(92)90143-K)
30. Illingworth JM, Williams PT (2012) Novel activated carbon fibre matting from biomass fibre waste. *Proc Inst Civil Eng Waste Resour Manag* 165:123–132. <https://doi.org/10.1680/warm.12.00001>

**Publisher's Note** Springer Nature remains neutral with regard to jurisdictional claims in published maps and institutional affiliations.